

**Characteristics of
water-vapour
inversions**

A. Devasthale et al.

**Characteristics of water-vapour
inversions observed over the Arctic by
Atmospheric Infrared Sounder (AIRS) and
radiosondes**

A. Devasthale¹, J. Sedlar¹, and M. Tjernström^{2,3}

¹Remote Sensing Division, Research Department, Swedish Meteorological and Hydrological Institute, Norrköping, Sweden

²Meteorological Institute, Stockholm University, Stockholm, Sweden

³Bert Bolin Centre for Climate Research, Stockholm University, Stockholm, Sweden

Received: 18 April 2011 – Accepted: 23 May 2011 – Published: 25 May 2011

Correspondence to: A. Devasthale (abhay.devasthale@smhi.se)

Published by Copernicus Publications on behalf of the European Geosciences Union.

Title Page

Abstract

Introduction

Conclusions

References

Tables

Figures

◀

▶

◀

▶

Back

Close

Full Screen / Esc

Printer-friendly Version

Interactive Discussion



Abstract

An accurate characterization of the vertical structure of the Arctic atmosphere is useful in climate change and attribution studies as well as for the climate modelling community to improve projections of future climate over this highly sensitive region. Here, we investigate one of the dominant features of the vertical structure of the Arctic atmosphere, i.e. water-vapour inversions, using eight years of Atmospheric Infrared Sounder data (2002–2010) and radiosounding profiles released from the two Arctic locations (North Slope of Alaska at Barrow and during SHEBA). We quantify the characteristics of clear-sky water vapour inversions in terms of their frequency of occurrence, strength and height covering the entire Arctic for the first time.

We found that the frequency of occurrence of water-vapour inversions is highest during winter and lowest during summer. The inversion strength is, however, higher during summer. The observed peaks in the median inversion-layer heights are higher during the winter half of the year, at around 850 hPa over most of the Arctic Ocean, Siberia and the Canadian Archipelago, while being around 925 hPa during most of the summer half of the year over the Arctic Ocean. The radiosounding profiles agree with the frequency, location and strength of water-vapour inversions in the Pacific sector of the Arctic. In addition, the radiosoundings indicate that multiple inversions are the norm with relatively few cases without inversions. The amount of precipitable water within the water-vapour inversion structures is estimated and we find a distinct, two-mode contribution to the total column precipitable water. These results suggest that water-vapour inversions are a significant source to the column thermodynamics, especially during the colder winter and spring seasons. We argue that these inversions are a robust metric to test the reproducibility of thermodynamics within climate models. An accurate statistical representation of water-vapour inversions in models would mean that the large-scale coupling of moisture transport, precipitation, temperature and water vapour vertical structure and radiation are also essentially captured well in such models.

Characteristics of water-vapour inversions

A. Devasthale et al.

Title Page

Abstract

Introduction

Conclusions

References

Tables

Figures



Back

Close

Full Screen / Esc

Printer-friendly Version

Interactive Discussion



1 Introduction

Water vapour is a prominent greenhouse gas that plays a key role in the regional and global hydrological cycle, and its positive feedback in a warming world is physically well understood (Bony et al., 2006). It is a dominant contributor to the present day total greenhouse effect, and its significant role is expected to remain so in the future (Schmidt et al., 2010). Water vapour has a well-defined zonal and vertical distribution, with a maximum in the tropics, secondary maxima at the mid-latitudes, while minima are observed in the polar regions. In the vertical it is typically at maximum near the surface. The variability in its zonal distribution is influenced by many factors but the temperature control of the saturation water-vapour partial pressure is the most important. This also controls the vertical structure. However, factors such as seasonality in the inter-tropical convergence zone, storm tracks, the movement of convective systems, to name a few, also play important roles.

In the Arctic, water vapour has a special significance (Curry et al., 1995) given its complex interplay with conditions unique to this region including: highly variable solar input, strong temperature inversions, sensitive clouds regimes, and the role of natural modes of variability such as Arctic Oscillation in the moisture transport. For example water-vapour inversions, i.e. when the water vapour increases with altitude, are often reported in association with dominant temperature inversions, especially in the inner Arctic (Tjernström et al., 2004; Sedlar et al., 2011). Water vapour typically has a near-surface maximum and decreases with altitude, due to the strong temperature control of its saturation pressure. In the Arctic, however, the dominant forcing by the near-surface climate combined with the large importance of meridional transport is expected to make water-vapour inversions common. There is clear evidence for the presence of humidity inversions from the ground based measurements taken at the northern high latitudes. For example, Serreze et al. (1995b) using a comprehensive rawinsonde dataset show persistent inversions during winter, especially over the inner Arctic. Gerding et al. (2004) using lidar measurements at Ny-Ålesund (79° N) report

Characteristics of water-vapour inversions

A. Devasthale et al.

Title Page

Abstract

Introduction

Conclusions

References

Tables

Figures



Back

Close

Full Screen / Esc

Printer-friendly Version

Interactive Discussion



Characteristics of water-vapour inversions

A. Devasthale et al.

Title Page

Abstract

Introduction

Conclusions

References

Tables

Figures

◀

▶

◀

▶

Back

Close

Full Screen / Esc

Printer-friendly Version

Interactive Discussion



case studies of WV MR (water-vapour mixing ratio) inversions at around 1.5 km in the atmosphere. Treffeisen et al. (2007) provide statistics on 15-years of humidity observations at the same site and present seasonality in the humidity inversions. Using data from the Arctic Ocean Experiment during summer 2001, Tjernström et al. (2004) report specific-humidity inversions also during summer over the inner Arctic; data from the Arctic Summer Cloud Ocean Study (ASCOS, Tjernström et al., 2011) confirms this result although summer moisture inversions are typically shallow. Sedlar et al. (2011) also report frequent specific-humidity inversions associated with low-level cloud cover from both central and pan-Arctic observational sites during all seasons and hypothesize on the importance of these for cloud-top location.

An increase of water vapour with altitude implies a larger downward component of the longwave radiation. Using profiles over a snow-covered glacier, Ohmura (2001) showed that approximately 90 % of the downwelling longwave radiation to the surface is emitted from a layer no deeper than 1000 m above the surface. Higher water vapour aloft also implies a downward transport towards the surface and contributes to keep the lowest troposphere at a very high relative humidity. Therefore it also contributes to the climatologically high cloud cover in the Arctic and can be seen as a manifestation of meridional water-vapour transport. In spite of its significance for the local meteorology, the characterization of water-vapour inversions in the Arctic remains limited to only a few locations (Serreze et al., 1995a, b; Gerding et al., 2004; Tjernström et al., 2004; Treffeisen et al., 2007). Satellite systems prior to 2002 were not capable of resolving the vertical structure of the Arctic atmosphere necessary for such studies although providing very useful information on the moisture budget (e.g. Groves and Francis, 2002). With the launch of the Atmospheric Infrared Sounder (AIRS) onboard NASA's Aqua satellite, the hyperspectral measurements from its hundreds of channels with strong and localized sensitivities to different layers of the atmosphere make it possible to investigate the vertical structure of water vapour covering the entire Arctic. The usability of AIRS over the Arctic region in studying various aspects is demonstrated in the previous works by Kay et al. (2008), Devasthale et al. (2010), and Pavelsky et

al. (2010), to name a few.

We tap in to this ability of AIRS and present the vertical structure of water vapour over the Arctic region. Here, we investigate the large-scale statistics of clear-sky water-vapour inversions and their seasonality for the first time. We also examine radiosounding profiles released from two Arctic locations in order to characterize water-vapour inversions for all-sky conditions with better vertical representation. The present study is organized with a presentation of the satellite and radiosounding data in Sect. 2, followed by a presentation and a discussion of the results in Sect. 3. Section 4 contains the conclusions and a discussion of the outlook for future work.

2 Data

2.1 The AIRS dataset

We use the retrieval of water-vapour (WV) mass mixing ratios (MRs) from Version 5 of the standard AIRS daily Level 3 products (Olsen et al., 2007a, b, c). These data are the summary of the best Level 2 data, ensuring that the dependence on apriori information is minimized. These Level 3 data are especially suitable for studying large-scale climatic features (Devasthale et al., 2010). The temperature and WV retrieval procedure makes use of roughly 2300 independent channels in the 3.7–15.4 μm spectral range, providing accurate estimates of WV MRs. A number of studies have validated the AIRS temperature and water-vapour retrievals, including over the high-latitude regions (cf. Divakarla et al., 2006; Fetzer et al., 2006; Gettelman et al., 2006).

We use data from both ascending (daytime) and descending (nighttime) passes of AIRS/Aqua for the eight-year period from June 2002 through May 2010. To investigate seasonality in the WV inversions, we examine winter (December through February, DJF), spring (March through May, MAM), summer (June through August, JJA) and autumn (September through November, SON) seasons separately. This is a too short time period for a climate dataset and will not capture potential effects of decadal oscil-

Characteristics of water-vapour inversions

A. Devasthale et al.

Title Page

Abstract

Introduction

Conclusions

References

Tables

Figures



Back

Close

Full Screen / Esc

Printer-friendly Version

Interactive Discussion



lations in the climate system. Specifically, it does not cover different phases of the main mode of variability in the Arctic, the Arctic Oscillation (AO). The AO was predominantly in its positive phase during the study period (2002–2010).

We use WV MRs at 1000, 925, 850, 700, 600, 500, and 400 hPa levels. For each profile, we examine the lowest level for which a valid retrieval is reported in the data. Using this level as a starting reference, we recursively search for an increase in WV MR in the overlying layers. If any of the layers above the reference level (up to 400 hPa) has a higher MR, a WV inversion is considered to be present. It is important to note here that the coarse resolution of the satellite data may miss weaker and/or shallower WV inversions, that might be picked up by other sensors, such as radiosoundings, and that this may bias the results in some seasons.

Using only those profiles that contain an inversion, we quantify the maximum inversion strength by taking the difference between the MR that has highest value and the MR at the reference level. We also examine pressure level at which the maximum WV MR occurs, the top of the WV inversion. The AIRS sensor cannot see through clouds and thus, in order to avoid contamination from clouds, only clear-sky cases are analysed. We, therefore, first examine the number of clear-sky observations and their spatial variations to investigate if they introduce any sampling artifact in the distributions of WV inversion frequency and strength (Fig. 1). The spatial pattern of the number of clear-sky observations is different in different seasons mainly governed by the seasonality in the cloud fraction. The cloud fraction is at minimum (maximum) in winter (summer) (Curry et al., 1996; Devasthale et al., 2011). Therefore, the total numbers of clear-sky observations are highest (lowest) during winter (summer).

2.2 Radiosoundings

Radiosoundings released twice daily, intermittently more frequently, from the North Slope of Alaska (NSA) Atmospheric Radiation Measurement (ARM) programmes station at Barrow as well as from the drifting Surface HEat Budget of the Arctic (SHEBA) ice camp are also analyzed. Radiosoundings from the NSA ARM site are released from

Characteristics of water-vapour inversions

A. Devasthale et al.

Title Page

Abstract

Introduction

Conclusions

References

Tables

Figures



Back

Close

Full Screen / Esc

Printer-friendly Version

Interactive Discussion



71.3° N 156.6° W, and we examine profiles from January 2003 to October 2009. The SHEBA ice camp drifted within 74.5 to 80.5° N and 143 to 168° W in the Beaufort and Chukchi Seas approximately a full year starting in October 1997. The approximate locations for radiosonde releases are shown in Fig. 1 (top-left panel). Note that SHEBA occurred long before the AIRS sensor was launched. There are 815 radiosounding profiles available from SHEBA and 3483 from Barrow.

While these profiles lack spatial resolution, they provide a significantly higher vertical resolution of thermodynamic properties than AIRS, at a temporal resolution similar to that of AIRS/Aqua overpasses. Additionally, the WV MRs are available regardless of sky conditions, increasing data quantity relative to AIRS/Aqua clear-sky only observations analyzed here. All radiosoundings are interpolated to a 100-m vertical grid, essentially filtering the higher-frequency variability while retaining the general larger-scale differential vertical advection of WV. Multiple WV inversions are common, so we examine only the inversion structure with the largest absolute WV MR. This tends to limit our analysis of WV inversions to the lowest inversion layer since WV MR varies with the temperature and pressure. Thus, we are inherently focusing our analysis on the portion of the atmosphere that is most important for the downwelling radiative fluxes (e.g. Ohmura, 2001). We simply exclude the characteristics of additional WV inversions within the profile when WV inversion statistics are computed. Water-vapour inversion strength is defined as the inversion-layer maximum MR minus the inversion-base MR, similar to the AIRS data analysis.

3 Results and discussions

3.1 Climatology of WV inversions from AIRS

Before examining and analysing the data, it is useful to summarize some of the factors and their interactions that may affect the WV inversion characteristics. Temperature inversion is one such factor that needs special consideration. The seasonality

Characteristics of water-vapour inversions

A. Devasthale et al.

Title Page

Abstract

Introduction

Conclusions

References

Tables

Figures



Back

Close

Full Screen / Esc

Printer-friendly Version

Interactive Discussion



Characteristics of water-vapour inversions

A. Devasthale et al.

Title Page

Abstract

Introduction

Conclusions

References

Tables

Figures

◀

▶

◀

▶

Back

Close

Full Screen / Esc

Printer-friendly Version

Interactive Discussion



in temperature-inversion strength has strong influence on the vertical mixing and the degree of coupling of the atmospheric boundary layer to the free troposphere. In the Arctic, the atmospheric boundary layer is partly decoupled from the free troposphere during large parts of the year. This decoupling is strongest during winter when solar radiation is absent and strong surface inversions often form in cloud-free conditions, and weakest during summer, when clouds are more frequent and solar radiation warms the surface (Kahl, 1990; Devasthale et al., 2010). The low-level atmospheric stability changes not only with the season, but also with the fraction of open water (Kay and Gettelman, 2009; Kay et al., 2011) and with the presence or absence of cloud cover (Persson et al., 2002; Sedlar et al., 2010). The large annual variability in solar radiation causes a large annual cycle in the near-surface temperature. Since the near-surface WV MR over snow and ice surfaces most often lies close to its saturation value (e.g. Andreas et al., 2002) this implies a large seasonal variability also in near-surface WV MR. The absolute WV MR is thus at a minimum during winter and a maximum during summer.

Another factor that influences WV inversions is the moisture transport to the Arctic from more southerly latitudes. A number of studies have addressed this issue in detail (Serreze et al., 1995b; Groves and Francis, 2002; Oshima and Yamazaki, 2004; Graversen et al., 2010; Jakobson and Vihma, 2010). The synthesis of the literature shows that moisture transport to the Arctic takes place during all seasons, although the relative magnitude differs from season-to-season. The two major transport pathways, from the North Atlantic and North Pacific oceans, are followed with transient moisture flux being the prime driver for the observed seasonality in the transport. The structure of the inversions, especially in winter, along with the often high relative humidity in the boundary layer combined with the Clausius-Clapeyron relationship contributes to the vertical structure of WV. In winter, the strong decoupling means that the transported WV often peaks above the inversion layer, while WV MR decreases towards the surface due to the decreasing temperature (Curry, 1983). Such a separation is more weakly present in summer.

Characteristics of water-vapour inversions

A. Devasthale et al.

Title Page

Abstract

Introduction

Conclusions

References

Tables

Figures

◀

▶

◀

▶

Back

Close

Full Screen / Esc

Printer-friendly Version

Interactive Discussion



The third important aspect is the role of natural modes of variability in controlling the Arctic atmosphere (Serreze et al., 1995b; Groves and Francis, 2002; Oshima and Yamazaki, 2004; Jakobson and Vihma, 2010). For example, it is shown that during positive phases of the Arctic Oscillation, the moisture transport across 70° N is enhanced up to six times during winter, compared to negative AO phase (Groves and Francis, 2002). While the meridional transport of moisture associated with a positive AO may certainly be larger at lower latitudes, the net flux into the Arctic across certain latitude also implies a convergence within the Arctic since the Earth, in a sense, “ends” at the pole.

All of these aspects shape the vertical distribution of WV over the Arctic and imply that the WV inversions would be expected to be more frequent in winter than in summer. This is indeed the case as displayed in Fig. 2, which shows the seasonal mean frequency of WV inversion occurrence using data from both the ascending and descending passes. It is calculated by dividing the number of profiles with a WV inversion detected by the total number of clear-sky profiles. Clearly, the frequency of occurrence is highest during winter and lowest during summer. The other two seasons seem to be in transition between these two modes, but with higher frequency of occurrence in spring than in autumn. In winter, the mean frequency is higher than 50 % over the Arctic Ocean. Two other regions also show a high frequency of occurrence; Siberia and the Canadian archipelago. In winter, the strongly decoupled clear-sky boundary layer has low WV MRs. Although the moisture is advected above the boundary layer mostly via two major pathways, i.e. from via North Atlantic and Pacific Oceans, the distribution of water vapour is rather homogeneous over the Arctic Ocean. Deposition of excess WV directly on the surface may also contribute to the frequency of the WV inversions. Ice precipitation contributes further to make the boundary layer even drier in an absolute sense (e.g. Blanchet and Girard, 1994; Curry et al., 1996). Therefore, the conditions for WV inversions are more conducive in winter, consistent with our clear-sky climatology.

In summer, the frequency is less than 10%. Near-surface temperatures in summer are higher and the relative increase in depth and turbulent mixing of the boundary layer can potentially increase the magnitude of WV MR over a potentially deeper layer. Additional latent heating associated with melting snow and ice at the surface also contributes to a relative increase in WV MR near the surface. As noted in the previous section, the coarse vertical resolution of the satellite data may contribute to an underestimation of summer WV-inversions if they are weaker and shallower. Still, the prevalence of moisture inversions even with the limitations of these data indicates that this is a very common feature in the Arctic atmosphere.

The areas around the Greenland, Iceland and Norwegian Seas have persistent cloud cover and also often have open ocean, increasing the potential for evaporation and increased moisture in the lower atmosphere. Both processes may contribute to the lowest inversion frequency values in those respective regions (Fig. 2). It is also to be noted that the phase of Arctic Oscillation was predominantly positive during the study period (2002–2010). This means that the moisture influx in to the Arctic was enhanced during the winter, contributing further to the favourable conditions for WV inversions.

Figure 3 shows the maximum median inversion strength (in g/kg) and its seasonality. The distributions of inversion strength are skewed and long-tailed and, therefore, its median values rather than the arithmetic means are shown. Since the WV inversion frequency is very low in summer, only few profiles are available to compute inversion-strength statistics. Therefore, the distribution shown in Fig. 3 in summer is very patchy. Nevertheless, the WV inversion strengths were generally largest during the summer relative to the rest of the year. The spatial pattern in the other seasons looks more robust. The winter season shows more pronounced inversion strengths compared spring and autumn. In general, the areas with high inversion frequency also show high inversion strength. Figure 4 shows the median pressure level at which the maximum WV MR was observed for the inversion cases. The observed peaks in inversion-peak height are higher during winter half of the year (December through May) at around 850 hPa over most of the Arctic Ocean, Siberia and the Canadian Archipelago. These results

Characteristics of water-vapour inversions

A. Devasthale et al.

[Title Page](#)[Abstract](#)[Introduction](#)[Conclusions](#)[References](#)[Tables](#)[Figures](#)[⏪](#)[⏩](#)[◀](#)[▶](#)[Back](#)[Close](#)[Full Screen / Esc](#)[Printer-friendly Version](#)[Interactive Discussion](#)

Characteristics of water-vapour inversions

A. Devasthale et al.

Title Page

Abstract

Introduction

Conclusions

References

Tables

Figures

◀

▶

◀

▶

Back

Close

Full Screen / Esc

Printer-friendly Version

Interactive Discussion



agree with the vertical locations of specific-humidity inversions in Serreze et al. (1995). Towards the summer months, the inversion-top height decreases. The maximum is around 925 hPa during most of the summer half of the year (June through November) over the Arctic Ocean. Such seasonal behaviour is in a way expected. For example, the temperature inversions are strong and tend to be geometrically thicker during winter (Kahl, 1990). Consequently, the moisture transport above this temperature inversion height will lead to vertically deeper WV inversions. In summer such deep surface inversions occur much more seldom. Additionally, cloud fraction is climatologically lowest in the Arctic during winter, and the interaction between clouds and radiation has been shown to be important for the boundary layer depth and vertical mixing potential (e.g. Sedlar et al., 2010). Thus, these clear-sky statistics may not capture the complete, all-sky thermodynamic structure of the Arctic atmosphere. The normalized histograms of pressure levels at which the peak in WV inversion was observed north of 70° N are shown in Fig. 5. In general most cases occur at or below 850 hPa with a distinct seasonality. In winter and spring roughly twice as many cases (55 and 65 %) occur at the 850 hPa level as at the lower 925 hPa level (24 and 35 %) while the opposite is the case for summer and autumn. The summer season has a particularly clear signal with a large majority of all cases (82 %) at the lower 925 hPa height.

Finally, note that the footprints of the spatio-temporal variations in the number of clear-sky observations (Fig. 1) are not visible in the composites of WV inversion frequency, strength and height (Figs. 2–4). This indicates that the results are to a first order not contaminated by analyzing only the clear-sky conditions hinting at the robustness of results shown here.

3.2 WV-inversion climatology from radiosoundings

To corroborate the results identified above, we examine the WV inversion characteristics from SHEBA and Barrow radiosoundings. Figures 6 and 7 show the seasonal relative frequency distribution (RFD, contours) of normalized WV MR as function of pressure (hPa) for SHEBA and Barrow, respectively. Normalized WV MR provides the

vertical location of largest absolute magnitude ($WV\ MR/WV\ MR_{max} = 1$) of WV MR within a profile. Here, this is used as a proxy for large-scale WV inversions. Consistent with the AIRS results, the maximum WV MRs tend to be found at higher altitude during winter and spring (Figs. 6 and 7a–b), compared to summer and autumn (Figs. 6 and 7c–d) for both locations. In winter, maximum WV MRs are generally found between 800 to 900 hPa. During spring, the maxima are also frequently found within this pressure range for SHEBA, but are slightly lower at Barrow. During summer and autumn, the increased mixing and boundary-layer depth result in the maximum WV MR to be found closer to the surface and slightly more well-mixed over a deeper layer for SHEBA (Fig. 6c–d). The differences in maximum WV MR during summer and autumn between SHEBA and Barrow may be a result of the air-mass origin, e.g. from open ocean, sea-ice covered ocean, or continental origin, and how the local vertical mixing is affected by the surface type (sea ice or land). Median profiles of normalized WVMR further confirm the seasonal differences in WV-inversion structure.

Figure 8 shows the total and seasonal RFDs for the number of WV inversions for SHEBA (Fig. 8a) and Barrow (Fig. 8b) profiles. Water-vapour inversions are a frequent phenomenon and occur in nearly all profiles. Up to 8 individual inversion layers are identified, thus the coarse vertical resolution of retrieved WVMRs from AIRS will miss a number of these vertical features. In the Beaufort Sea region of the Arctic, 2 to 4 WV inversions occur most frequently.

The RFDs of pressure level of the maximum WV MR within the inversion layer are shown in Fig. 8c–d. To reiterate, only characteristics from the WV inversion with the maximum WV MR are included in Fig. 8c–f statistics. These histograms show the maximum WV MR occurs generally between 800 to 1000 hPa, in broad agreement with the AIRS Arctic-wide inversion maxima levels and Figs. 6–7. The maximum WV MRs are observed at lower pressures (higher) during winter and spring at SHEBA, while at Barrow the pressures were lower only during spring. However, although the seasonal differences agree well with the AIRS data, the level of maximum WVMR is generally lower in the soundings than in the satellite data. It is not possible to say if this

Characteristics of water-vapour inversions

A. Devasthale et al.

[Title Page](#)[Abstract](#)[Introduction](#)[Conclusions](#)[References](#)[Tables](#)[Figures](#)[Back](#)[Close](#)[Full Screen / Esc](#)[Printer-friendly Version](#)[Interactive Discussion](#)

indicates a systematic difference or is due to the fact that the soundings also include cloudy cases. Due to the vertical resolution of the satellite data, it is possible that stronger inversions are missed between the 1000 to 925 hPa levels, but are captured by the radiosoundings.

In general, WV inversion strengths are positively skewed (Fig. 8e–f), although strengths ranging 0.2–0.5 g/kg are most frequent. Again, this range of inversion strength agrees with median statistics from AIRS data. Slightly broader peaks are observed during both winter and spring for SHEBA and Barrow, which suggests that stronger inversions occur more frequently. The long, positive tails of the RFDs emerge mainly from stronger inversions during summer (Fig. 8e–f, red lines). This increases confidence that the increased inversion strength observed by AIRS during summer may be a common feature of the summertime thermodynamics and not an artifact of data reduction.

Since the radiosounding profiles are analyzed regardless of cloudiness, it is possible that cloud processing may impact the presence and/or strength of WV inversions. Considering the relatively low magnitudes of cloud liquid- and ice-water content observed for Arctic clouds (Shupe et al., 2001, 2008; Sedlar et al., 2010), we argue that the cloud detrainment of liquid and ice water alone cannot explain the inversion strengths observed by the radiosoundings. Instead, large-scale advection of WV appears to be the primary mechanism for the inversion structures. However, Sedlar et al. (2011) find that the presence of WV inversions, particularly when coinciding with temperature inversions, is an important mechanism for cloud formation and lifetime in the Arctic.

3.3 WV inversion contributions to total column water

The vertical location and absolute strength of inversions may play an important role in radiative and cloud-formation processes in the lower atmosphere. Atmospheric precipitable water (PW) is the total amount of condensed water vapour along a vertical path. Zhang et al. (2001) have shown that the atmospheric downwelling longwave flux increases logarithmically with PW and show a robust relationship between snow melt

Characteristics of water-vapour inversions

A. Devasthale et al.

Title Page

Abstract

Introduction

Conclusions

References

Tables

Figures



Back

Close

Full Screen / Esc

Printer-friendly Version

Interactive Discussion



and total PW. Here we estimate the importance of WV inversions to the total column PW (in cm) calculated by integrating the WV vertically by:

$$PW = \int_{z_1}^{z_2} \rho_a \cdot \omega_v \cdot dz \quad (1)$$

where z is height level, ρ_a is the air density and ω_v the WV MR. For total PW, we integrate Eq. (1) from the surface to 10 km above the surface. The PW estimate is not a true column-integrated value from a single spatial location. However, we make a general assumption to justify this approach. First, we assume that the majority of total PW is found in the lower atmosphere where temperatures are higher. We then assume that the time scale is shorter for the radiosounding to ascend past approximately the 800 hPa level, where the majority of inversions are found, than the time scale for thermodynamic changes through large-scale advection. Thus our measure of total PW is assumed to be representative of the lower Arctic atmosphere, where also the majority of WV MR maxima are observed (Figs. 6–8). Analysis of the integrated total PW shows good agreement with independent surface-based microwave radiometers at both sites in terms of absolute magnitudes and the seasonal cycle (not shown). Additionally, we calculate the partial PW for the maximum WV inversion layers by integrating Eq. (1) from each inversion base to top (level of maximum WV MR).

In Fig. 9, the integrated partial PW across the inversion is normalized by the total PW and shown as a function of total PW. Comparing the contribution of the maximum WV inversion to the total PW, we find two apparent regimes. For relatively low values of total PW, the inversion often contributes up to 40 % of the total column PW and reaches above 50 % for some cases. When the total PW is relatively large, the inversion contribution is lower and often less than 15 % of the total. The L-shaped relationship between PW from inversions and total PW suggests that WV inversions can have a potentially significant impact on the longwave radiative characteristics of the atmosphere. This is especially true during the winter and spring seasons when temperatures are generally colder relative to summer and autumn considering the dependence of WV MR on temperature and pressure. Under cloud-free conditions, the enhanced WV advection

Characteristics of water-vapour inversions

A. Devasthale et al.

Title Page

Abstract

Introduction

Conclusions

References

Tables

Figures

◀

▶

◀

▶

Back

Close

Full Screen / Esc

Printer-friendly Version

Interactive Discussion



associated with the inversion may impact the atmospheric emissivity. Potentially, the emissivity changes could lead to sufficient longwave radiative cooling and diabatically introduce thermodynamic stability changes or lead to condensation and cloud formation (Curry, 1983), provided cloud condensation or ice nuclei particles are present and the large-scale meteorology supports cloud formation.

4 Conclusions

The Arctic atmosphere is unique in many ways and is the result of several geophysical variables interacting with each other in a complex manner. The need for an accurate characterization of the vertical structure of the Arctic is increasingly relevant as such information is extremely useful in climate change and attribution studies, as well as for the climate modelling community to improve projections of the future climate over this susceptible region. Among the dominant features of the Arctic atmosphere, the one that is least studied so far is the water-vapour vertical structure and inversions in its vertical distribution. Using eight years of data from June 2002 till May 2010 from the AIRS instrument, we quantified the characteristics of clear-sky water-vapour inversions in terms of frequency of occurrence, strength and height covering the entire Arctic. We also discussed the seasonality in these characteristics. We complemented the spatial characteristics observed by satellite with enhanced vertical resolution, all-sky characteristics observed from radiosoundings released from two Arctic sites.

We found that:

- The frequency of occurrence of WV inversions is highest during winter and lowest during summer. The other two seasons seem to be the transition between these two modes. In winter, the frequency is much higher than 50 % for cloud free conditions over the Arctic Ocean on average. The other two regions that also show high frequency of occurrence are Siberia and the Canadian archipelago. In summer, the corresponding frequency is less than 10 %, however these frequencies may be biased low by the vertical resolution of satellite profiles

Characteristics of water-vapour inversions

A. Devasthale et al.

Title Page

Abstract

Introduction

Conclusions

References

Tables

Figures



Back

Close

Full Screen / Esc

Printer-friendly Version

Interactive Discussion



- Radiosounding profiles indicate that water-vapour inversions are almost always present, and the occurrence of no inversions occurred primarily during the autumn at Barrow. Multiple inversions are much more common than single-inversion layers.
- The winter and spring seasons show pronounced inversion strength in locations where inversion occurrence was most frequent. Summer inversion strengths were found to be largest. The radiosoundings also suggests that the strongest inversion strengths tend to be found during summer when temperatures are the highest, however the inversion strengths were most often between 0.2–0.5 g/kg for all seasons.
- The observed peaks in the median inversion-layer heights are higher during the winter half-year at around 850 hPa over most of the Arctic Ocean, Siberia and the Canadian Archipelago. In most of the summer half-year they are lower, at around 925 hPa over the Arctic Ocean. Radiosounding inversion structures agree with these seasonal vertical distributions.
- The lack of clear correlation between the spatio-temporal variations in the number of clear-sky observations and the composites of WV inversion frequency and strength, lends credibility to the results.
- The contribution of the maximum WV inversion to the total column precipitable water is shown to be dependent on the background thermodynamics. When total precipitable water is relatively low, the water-vapour inversion can contribute by up to 40 %, and occasionally higher, of the total column value. When total precipitable water is relatively high, the maximum inversion structure contributes generally less than 15 %. Therefore the impact of WV inversions on the radiative characteristics of the atmosphere is largest during the winter and spring seasons, which are the seasons when cloud fraction is generally lowest (e.g. Curry et al., 1996).

Characteristics of water-vapour inversions

A. Devasthale et al.

Title Page

Abstract

Introduction

Conclusions

References

Tables

Figures

◀

▶

◀

▶

Back

Close

Full Screen / Esc

Printer-friendly Version

Interactive Discussion



Characteristics of water-vapour inversions

A. Devasthale et al.

Title Page

Abstract

Introduction

Conclusions

References

Tables

Figures

◀

▶

◀

▶

Back

Close

Full Screen / Esc

Printer-friendly Version

Interactive Discussion



Global and regional climate models should be able to reproduce similar features in order to test the fidelity of statistics derived from them. Given the complex nature and various aspects that shape WV inversions, it is a good metric to test the models. An accurate statistical representation of WV inversions in models would mean that the large-scale coupling of moisture transport, the temperature and water-vapour vertical structure and radiation is also essentially captured well in such models. In such an evaluation, however, it is important to filter the model data through the satellite weighting functions in order to get a comparable result.

Acknowledgements. We would like to acknowledge the AIRS Science Team and NASA's GES DISC for their efforts in making AIRS data freely available for research. We would also like to acknowledge invaluable efforts of those maintaining data at Barrow and SHEBA. This work was supported by the Swedish National Space Board.

References

- Andreas, E. L., Guest, P. S., Persson, P. O. G., Fairall, C. W., Horst, T. W., Moritz, R. E., and Semmer, S. R.: Near-surface water vapor over polar sea ice is always near ice saturation. *J. Geophys. Res.*, 107(C10), 8033, doi:10.1029/2000JC000411, 2002.
- Blanchet, J.-P. and Girard, E.: Arctic greenhouse cooling, *Nature*, 371, p. 383, 1995.
- Bony, S., Colman, R., Kattsov, V. M., Allan, R. P., Bretherton, C. S., Dufresne, J.-L., Hall, A., Hallegatte, S., Holland, M. M., Ingram, W., Randall, D. A., Soden, B. J., Tselioudis, G., and Webb, M. J.: How Well Do We Understand and Evaluate Climate Change Feedback Processes?, *J. Climate*, 19, 3445–3482, 2006.
- Curry, J. A.: On the Formation of Continental Polar Air, *J. Atmos. Sci.*, 40, 2278–2292, 1983.
- Curry, J. A., Schramm, J. L., Serreze, M. C., and Abert, E. E.: Water vapor feedback over the Arctic Ocean, *J. Geophys. Res.*, 100(D7), 223–229, 1995.
- Curry, J. A., Rossow, W. B., Randall, D., and Schramm, J. L.: Overview of Arctic Cloud and Radiation Characteristics, *J. Clim.*, 9, 1731–1764, 1996.
- Devasthale, A., Tjernström, M., Karlsson, K.-G., Thomas, M. A., Jones, C., Sedlar, J., and Omar, A. H.: The vertical distribution of thin features over the Arctic analysed from CALIPSO observations. Part I: Optically thin clouds, *Tellus B*, 63(1), 77–85, 2011.

**Characteristics of
water-vapour
inversions**

A. Devasthale et al.

[Title Page](#)[Abstract](#)[Introduction](#)[Conclusions](#)[References](#)[Tables](#)[Figures](#)[◀](#)[▶](#)[◀](#)[▶](#)[Back](#)[Close](#)[Full Screen / Esc](#)[Printer-friendly Version](#)[Interactive Discussion](#)

Devasthale, A., Willen, U., Karlsson, K.-G., and Jones, C. G.: Quantifying the clear-sky temperature inversion frequency and strength over the Arctic Ocean during summer and winter seasons from AIRS profiles, *Atmos. Chem. Phys.*, 10, 5565–5572, doi:10.5194/acp-10-5565-2010, 2010.

5 Divakarla, M. G., Barnet, C. D., Goldberg, M. D., McMillin, L. M., Maddy, E., Wolf, W., Zhou, L., and Liu, X.: Validation of Atmospheric Infrared Sounder temperature and water vapor retrievals with matched radiosonde measurements and forecasts, *J. Geophys. Res.*, 111, D09S15, doi:10.1029/2005JD006116, 2006.

Fetzer, E. J.: Preface to special section: Validation of Atmospheric Infrared Sounder Observations, *J. Geophys. Res.*, 111, D09S01, doi:10.1029/2005JD007020, 2006.

10 Gerding, M., Ritter, C., Mueller, M., and Nueber, R.: Tropospheric water vapour soundings by lidar at high Arctic latitudes, *Atmos. Res.*, 71, 289–302, 2004.

Gettelman, A., Walden, V. P., Miloshevich, L. M., Roth, W. L., and Halter, B.: Relative humidity over Antarctica from radiosondes, satellites, and a general circulation model, *J. Geophys. Res.*, 111, D09S13, doi:10.1029/2005JD006636, 2006

15 Graversen, R. G., Mauritsen, T., Drijfhout, S., Tjernström, M., and Mårtensson, S.: Warm winds from the Pacific caused extensive Arctic sea-ice melt in summer 2007, *Clim. Dynam.*, 0930-7575, doi:10.1007/s00382-010-0809-z, 2010.

Groves, D. G. and Francis, J. A.: Variability of the Arctic atmospheric moisture budget from TOVS satellite data, *J. Geophys. Res.*, 107(D24), 4785–4800, 2002.

20 Jakobson, E. and Vihma, T.: Atmospheric moisture budget in the Arctic based on the ERA-40 reanalysis, *Int. J. Climatol.*, 30, 14, 2175–2194, 2010.

Kahl, J. D.: Characteristics of the Low-Level Temperature Inversion Along the Alaskan Arctic Coast, *Int. J. Climatol.*, 10, 537–548, 1990.

25 Kay, J. E., L'Ecuyer, T., Gettelman, A., Stephens, G., and O'Dell, C.: The contribution of cloud and radiation anomalies to the 2007 Arctic sea ice extent minimum, *Geophys. Res. Lett.*, 35, L08503, doi:10.1029/2008GL033451, 2008.

Kay, J. E. and Gettelman, A.: Cloud influence on and response to seasonal Arctic sea ice loss, *J. Geophys. Res.*, Atmos., D18204, doi:10.1029/2009JD011773, 2009.

30 Kay, J. E., Raeder, K., Gettelman, A., and Anderson, J.: The boundary layer response to recent Arctic sea ice loss and implications for high-latitude climate feedbacks, *J. Climate*, 24, 428–447, doi:10.1175/2010JCLI3651.1, 2011.

Ohumura, A.: Physical Basis for the Temperature-Based Melt-Index Method, *J. Appl. Meteorol.*,

Characteristics of water-vapour inversions

A. Devasthale et al.

Title Page

Abstract

Introduction

Conclusions

References

Tables

Figures

◀

▶

◀

▶

Back

Close

Full Screen / Esc

Printer-friendly Version

Interactive Discussion



40, 753–761, 2001.

Olsen, E. T., Susskind, J., Blaisdell, J., and Rosenkranz, P.: AIRS/AMSU/HSB Version 5 Level 2 Quality Control and Error Estimation, JPL, Pasadena, USA, 15 pp., 2007a.

Olsen, E. T., Granger, S., Manning, E., and Blaisdell, J.: AIRS/AMSU/HSB Version 5 Level 3 Quick Start, JPL, Pasadena, USA, 25 pp., 2007b.

Olsen, E. T., Fishbein, E., Hearty, T., Lee, S.-Y., Irion, F. W., Kahn, B., Manning, E., Blaisdell, J., Susskind, J., Iredell, L., Barnet, C., Maddy, E., Rosenkranz, P., McMillan, W. W., Sergio DeSouza-Machado, and Knuteson, R.: AIRS Version 5 release Level 2 standard product quick start, JPL, Pasadena, USA, 67 pp., 2007c.

Oshima, K. and Yamazaki, K.: Seasonal variation of moisture transport in polar regions and the relation with annular modes, *Polar Meteorol. Glaciol.*, 18, 30–53, 2004.

Pavelsky, T. M., Boé, J., Hall, A., and Fetzer, E. J.: Atmospheric inversion strength over polar oceans in winter regulated by sea ice, *Clim. Dynam.*, 36(5–6), 945–955, doi:10.1007/s00382-010-0756-8, 2010.

Persson, P. O. G., Fairall, C. W., Andreas, E. L., Guest, P. S., and Perovich, D. K.: Measurements near the Atmospheric Surface Flux Group tower at SHEBA, Near-surface conditions and surface energy budget, *J. Geophys. Res.*, 107(C10), 8045, doi:10.1029/2000JC000705, 2002.

Schmidt, G. A., Ruedy, R. A., Miller, R. L., and Lacis, A. A.: Attribution of the present-day total greenhouse effect, *J. Geophys. Res.*, 115, D20106, doi:10.1029/2010JD014287, 2010.

Sedlar, J. and Tjernström, M.: Stratiform Cloud – Inversion Characterization During the Arctic Melt Season, *Bound.-Layer Meteorol.*, 132, 455–474, doi:10.1007/s10546-009-9407-1, 2009.

Sedlar, J., Tjernström, M., Maurtisten, T., Shupe, M. D., Brooks, I. M., Persson, P. O. G., Birch, C. E., Leck, C., Sirevaag, A., and Nicolaus, M.: A transitioning Arctic surface energy budget: the impacts of solar zenith angle, surface albedo and cloud radiative forcing, *Clim. Dynam.*, 11, doi:10.1007/s00382-010-0937-5, 2010.

Sedlar, J., Shupe, M. D., and Tjernström, M.: On the relationship between thermodynamic structure and cloud top, and its climate significance in the Arctic, *J. Climate*, submitted, 2011.

Serreze, M. C., Barry, R. G., and Walsh, J. E.: Atmospheric water vapor characteristics at 70N, *J. Climate*, 8, 719–731, 1995a.

Serreze, M. C., Rehder, M. C., Barry, R. G., Kahl, J. D., and Zaitseva, N. A.: The distribution and

transport of atmospheric water vapour over the Arctic basin, *Int. J. Climatol.*, 15, 709–727, 1995b.

Tjernström, M., Leck, C., Ola, P., Persson, G., Jensen, M. L., Oncley, S. P., and Targino, A.: The summertime Arctic atmosphere, *B. Am. Meteorol. Soc.*, 1305–1321, 2004.

- 5 Treffeisen, R., Krejci, R., Ström, J., Engvall, A. C., Herber, A., and Thomason, L.: Humidity observations in the Arctic troposphere over Ny-Ålesund, Svalbard based on 15 years of radiosonde data, *Atmos. Chem. Phys.*, 7, 2721–2732, doi:10.5194/acp-7-2721-2007, 2007.

Characteristics of water-vapour inversions

A. Devasthale et al.

Title Page

Abstract

Introduction

Conclusions

References

Tables

Figures

⏪

⏩

◀

▶

Back

Close

Full Screen / Esc

Printer-friendly Version

Interactive Discussion



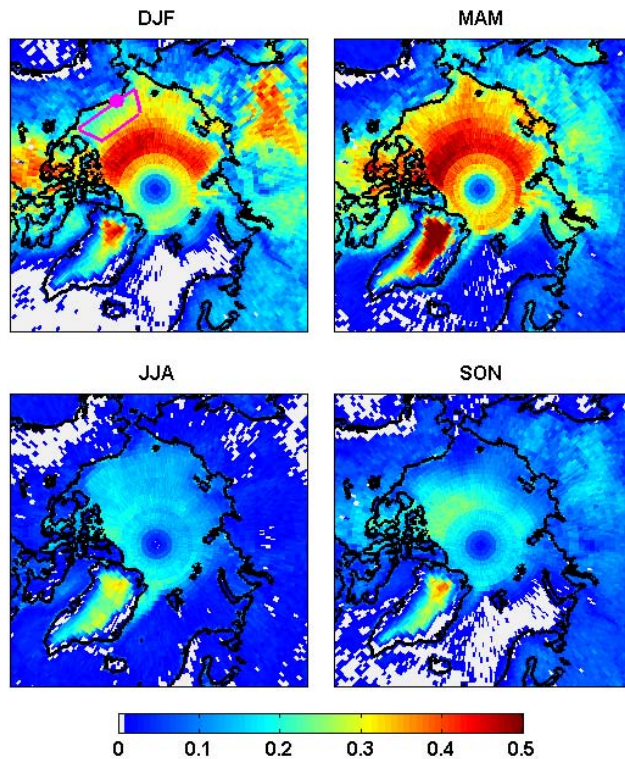


Fig. 1. Fraction of clear-sky observations available for analysis during the 2002–2010 period. The small circle and trapezoid in magenta colour denote the locations of Barrow station and SHEBA area respectively.

Characteristics of water-vapour inversions

A. Devasthale et al.

Title Page

Abstract Introduction

Conclusions References

Tables Figures

◀ ▶

◀ ▶

Back Close

Full Screen / Esc

Printer-friendly Version

Interactive Discussion



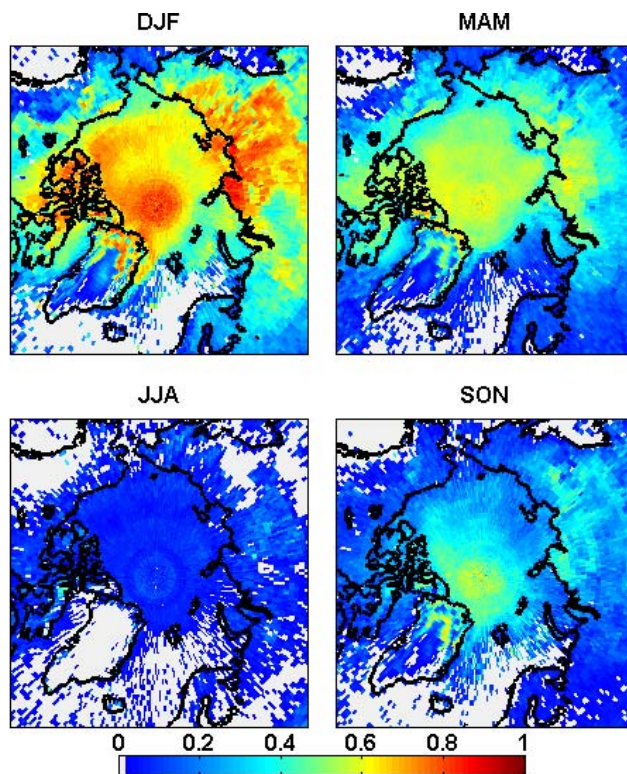


Fig. 2. Seasonal mean frequency of occurrence of WV inversions. The data from 2002–2010 are used for the analysis. The data for both ascending and descending passes are used for computing averages.

Characteristics of water-vapour inversions

A. Devasthale et al.

Title Page

Abstract Introduction

Conclusions References

Tables Figures

◀ ▶

◀ ▶

Back Close

Full Screen / Esc

Printer-friendly Version

Interactive Discussion



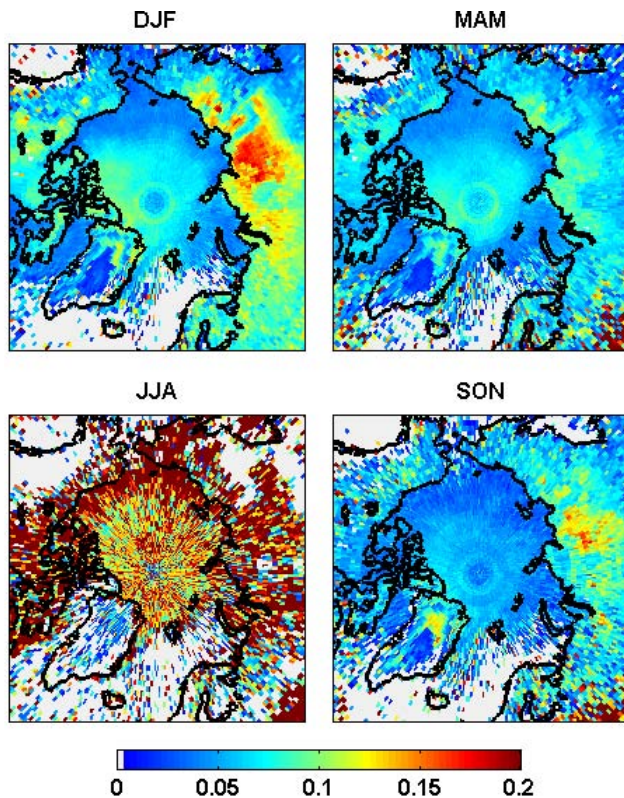


Fig. 3. Median water-vapour inversion strength (in g/kg) and its seasonality.

Characteristics of water-vapour inversions

A. Devasthale et al.

Title Page

Abstract Introduction

Conclusions References

Tables Figures

◀ ▶

◀ ▶

Back Close

Full Screen / Esc

Printer-friendly Version

Interactive Discussion



**Characteristics of
water-vapour
inversions**

A. Devasthale et al.

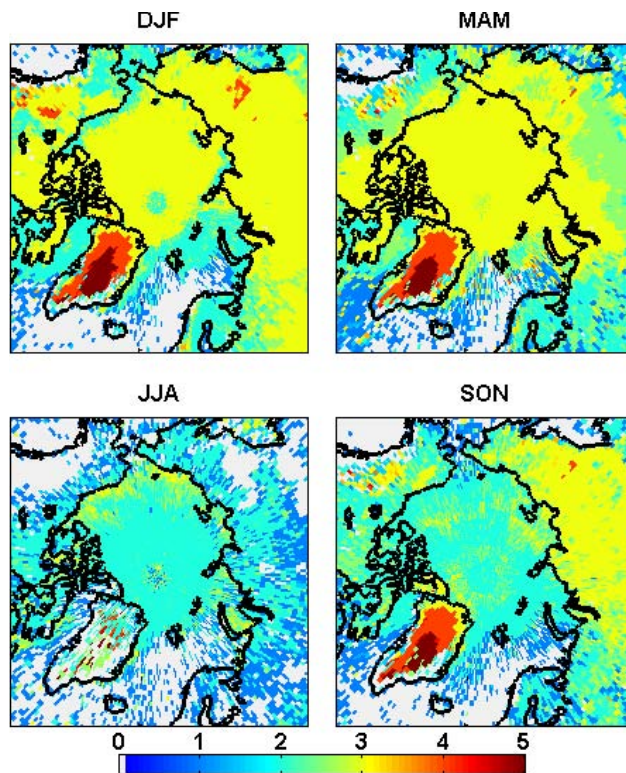


Fig. 4. Median pressure level at which peak in WV inversion was observed. 1–1000 hPa, 2–925 hPa, 3–850 hPa, 4–700 hPa, 5–600 hPa and above.

[Title Page](#)[Abstract](#)[Introduction](#)[Conclusions](#)[References](#)[Tables](#)[Figures](#)[◀](#)[▶](#)[◀](#)[▶](#)[Back](#)[Close](#)[Full Screen / Esc](#)[Printer-friendly Version](#)[Interactive Discussion](#)

**Characteristics of
water-vapour
inversions**

A. Devasthale et al.

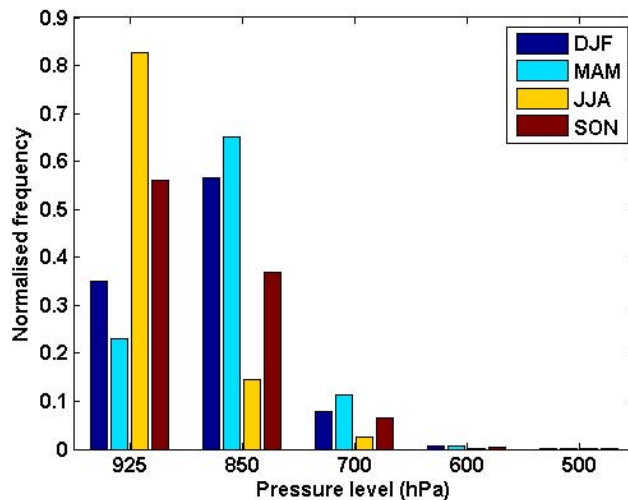


Fig. 5. The normalized histograms of pressure levels at which the peak in WV inversion was observed over 70° N–90° N, 180° W–180° E.

[Title Page](#)[Abstract](#)[Introduction](#)[Conclusions](#)[References](#)[Tables](#)[Figures](#)[◀](#)[▶](#)[◀](#)[▶](#)[Back](#)[Close](#)[Full Screen / Esc](#)[Printer-friendly Version](#)[Interactive Discussion](#)

**Characteristics of
water-vapour
inversions**

A. Devasthale et al.

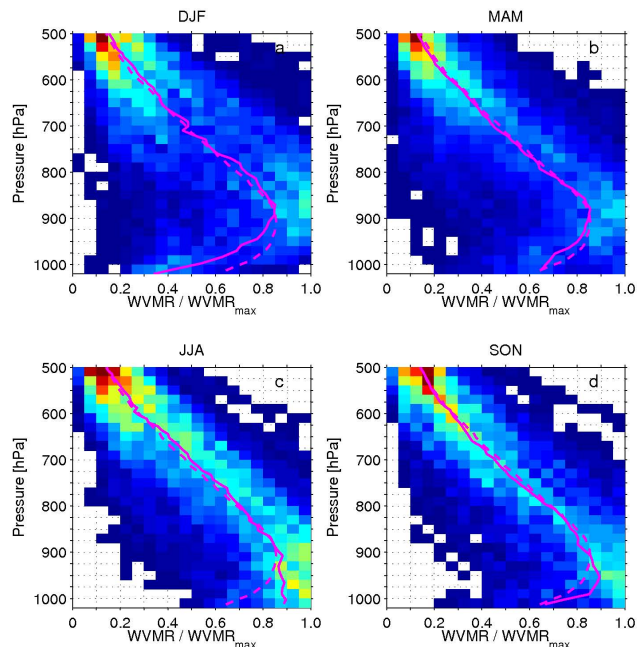


Fig. 6. SHEBA seasonal radiosounding RFDs [contours, warmer colors indicate increasing frequency] of the vertical distribution (hPa) of the WVMR normalized by the profile maximum WVMR for —bf(a) DJF, (b) MAM, (c) JJA and (d) SON. The seasonal median normalized WVMR (magenta line) and the median for all profiles (magenta dashed) are included.

Title Page

Abstract

Introduction

Conclusions

References

Tables

Figures

◀

▶

◀

▶

Back

Close

Full Screen / Esc

Printer-friendly Version

Interactive Discussion



**Characteristics of
water-vapour
inversions**

A. Devasthale et al.

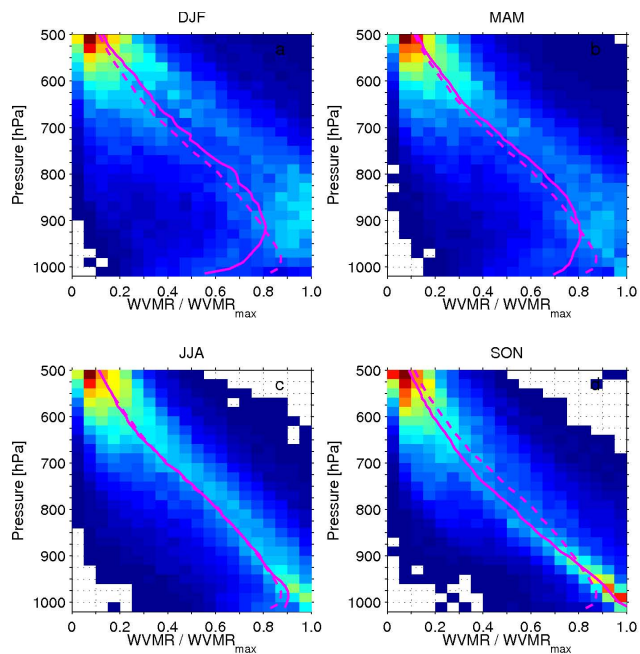


Fig. 7. Same as in Fig. 6, but for Barrow radiosoundings from January 2003 to October 2009.

[Title Page](#)[Abstract](#)[Introduction](#)[Conclusions](#)[References](#)[Tables](#)[Figures](#)[◀](#)[▶](#)[◀](#)[▶](#)[Back](#)[Close](#)[Full Screen / Esc](#)[Printer-friendly Version](#)[Interactive Discussion](#)

Characteristics of water-vapour inversions

A. Devasthale et al.

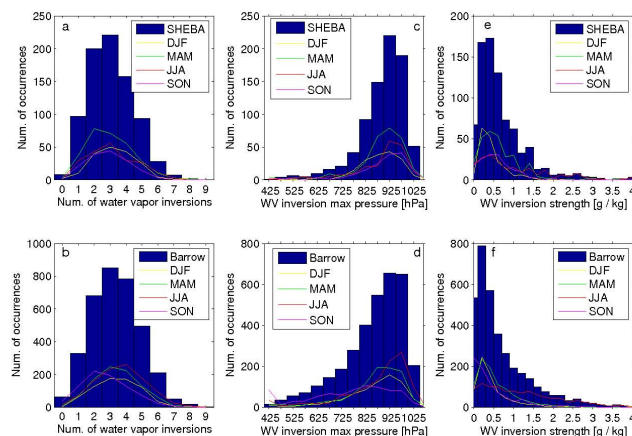


Fig. 8. The total (bars) and seasonal (lines) RFDs of (a–b) the total number of WV inversions identified; (c–d) The vertical pressure level [hPa] of the maximum WVMR for the inversion structure containing the largest absolute WVMR; (e–f) The inversion strength (g kg^{-1}) of the inversion structure containing the largest absolute WVMR. SHEBA statistics are on the top row while Barrow's are on the lower row.

Title Page

Abstract

Introduction

Conclusions

References

Tables

Figures

◀

▶

◀

▶

Back

Close

Full Screen / Esc

Printer-friendly Version

Interactive Discussion



Characteristics of water-vapour inversions

A. Devasthale et al.

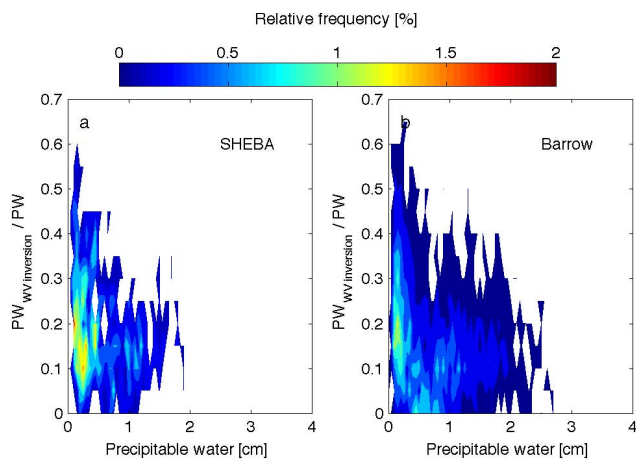


Fig. 9. The RFDs of maximum WV inversion structure PW ($PW_{WV\ Inversion}$) normalized by the total column PW as a function total column PW (in cm) for **(a)** SHEBA **(b)** Barrow radiosounding profiles.

[Title Page](#)[Abstract](#)[Introduction](#)[Conclusions](#)[References](#)[Tables](#)[Figures](#)[◀](#)[▶](#)[◀](#)[▶](#)[Back](#)[Close](#)[Full Screen / Esc](#)[Printer-friendly Version](#)[Interactive Discussion](#)